

Motion of nanodroplets near chemical heterogeneities

A. Moosavi, M. Rauscher, and S. Dietrich

*Max-Planck-Institut für Metallforschung, Heisenbergstr. 3, D-70569 Stuttgart, Germany, and
Institut für Theoretische und Angewandte Physik,
Universität Stuttgart, Pfaffenwaldring 57, D-70569 Stuttgart, Germany*

(Dated: November 16, 2018)

We investigate the dynamics of nanoscale droplets in the vicinity of chemical steps which separate parts of a substrate with different wettabilities. Due to long-ranged dispersion forces, nanodroplets positioned on one side of the step perceive the different character of the other side even at some distances from the step, leading to a dynamic response. The direction of the ensuing motion of such droplets does not only depend on the difference between the equilibrium contact angles on these two parts but in particular on the difference between the corresponding Hamaker constants. Therefore the motion is not necessarily directed towards the more wettable side and can also be different from that of droplets which span the step.

The interest in dynamical wetting phenomena has increased significantly with the development of micro- and nanofluidic systems, which allow one to handle minute amounts of liquid containing, e.g., DNA or proteins for chemical analysis and biotechnology [1, 2]. In particular chemically heterogeneous systems with tailored, spatially varying wetting properties have found important applications in this context [3, 4]. In open microfluidic systems, fluids are transported on chemical channels, i.e., lyophilic stripes embedded in lyophobic substrates. While present devices are based mostly on micron sized channels, further miniaturization down to the nanoscale is clearly on the roadmap. This will eventually lead to nanofluidic systems for which a variety of physical phenomena, which on the microscale and above are either irrelevant or summarized into boundary conditions, become important [5, 6]. For the optimization of the performance of nanofluidic systems it is critical to understand the basic fluidic issues occurring on those scales. Recent theoretical studies of nanoscale fluids on chemically [7] and topographically [8] structured substrates have underscored the importance of such investigations.

Those analytical tools [9, 10, 11, 12] which rely on classical macroscopic theory are not adequate for this purpose. Apart from some molecular dynamics simulations [7, 13], which are computationally demanding, to a large extent the available numerical investigations are based on solving thin film equations [14, 15, 16, 17, 18]. In most of these studies the chemical heterogeneities are introduced via abrupt, lateral changes of those parameters which characterize the potentials of homogenous substrates [14, 16, 17]. However, this does not capture the actual behavior of such substrate potentials, even if the underlying chemical steps are taken to be atomically sharp [19]. Smooth chemical heterogeneities have been studied in Ref. [18] by introducing a continuously varying Hamaker constant. But this approach is only applicable for very smooth variations of the wetting properties. Studies of the dynamics of droplets in the vicinity of topographic steps have shown that on the nanoscale a detailed modeling of the substrate and thus of the resulting effective interface potential is mandatory [8]. For a chem-

ical step, this has been worked out within the framework of microscopic density functional theory with a view on the morphology of static wetting films [20, 21, 22].

Here we study the dynamics of nanodroplets in the vicinity of chemical steps, i.e., sharp and straight boundaries between two parts of a substrate with different wetting properties. Such steps appear in open micro- and nanofluidic systems as the edges of chemical channels. As a paradigmatic case we focus on a chemical step formed by two adjacent quarter spaces composed of different substrate particles. We analyze the driving force on the droplets and perform numerical calculations

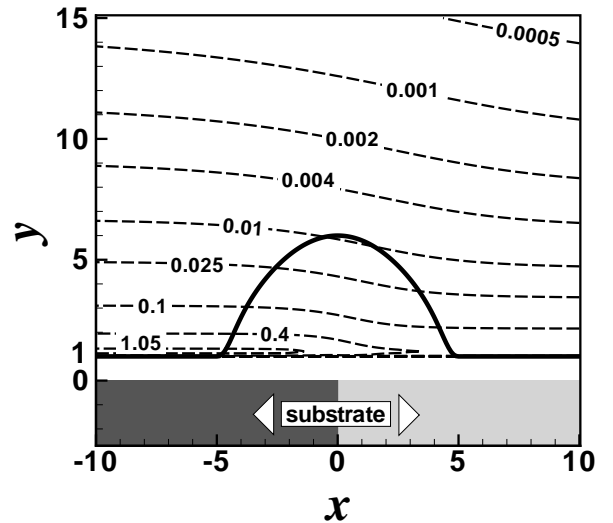


FIG. 1: The chemical step is translationally invariant along the z axis (orthogonal to the image plane). A nanodroplet (full line) is exposed to the vertically and laterally varying DJP, the contour plot of which is shown. Here both sides of the substrate are taken to correspond to the \ominus case with $b^{\triangleleft} = b^{\triangleleft}$ and $\theta_{eq}^{\triangleleft} = 97.2^\circ$ ($B^{\triangleleft} = 0$, $C^{\triangleleft} = 3$) and $\theta_{eq}^{\triangleleft} = 51.3^\circ$ ($B^{\triangleleft} = 0$, $C^{\triangleleft} = 1$) [see Eqs. (3) and (4) and the main text]. Lengths are measured in units of b^{\triangleleft} (see the main text). A coating of the substrate is not indicated as here $B^{\triangleleft} = B^{\triangleleft} = 0$ so that for $x \rightarrow \pm\infty$ the equilibrium thicknesses of the underlying film are the same, i.e., $y_0^{\triangleleft} = y_0^{\triangleleft} = y_0 = b^{\triangleleft}$.

employing the standard boundary integral method for hydrodynamic Stokes flow providing the underlying dynamics.

As depicted in Fig. 1 we consider a partially wetting, non-volatile, and incompressible liquid forming a nanodroplet on top of a precursor wetting film over a chemical step. The type of chemical step which we consider here can be viewed as being composed of two different quarter spaces with each of the two corresponding upper surfaces coated additionally with a thin layer of different materials. Accordingly, as a basic element we first consider an edge without surface coating, say the left part of the substrate shown in Fig. 1 which we denote by the superscript \triangleleft . Assuming Lennard-Jones type intermolecular pair potentials $V_{\alpha\beta}(r) = M_{\alpha\beta}/r^{12} - N_{\alpha\beta}/r^6$, where $M_{\alpha\beta}$ and $N_{\alpha\beta}$ are material parameters, and α and β relate to liquid (l), substrate (s), or coating (c) particles, the local disjoining pressure (DJP) corresponding to an edge occupying $\Omega_s^{\triangleleft} = \{\mathbf{r} \in \mathbb{R}^3 \mid x \leq 0, y \leq 0, z \in \mathbb{R}\}$ is given by [23]

$$\Pi_e^{\triangleleft}(x, y) = \int_{\Omega_s^{\triangleleft}} \frac{\Delta M^{\triangleleft}}{|\mathbf{r} - \mathbf{r}'|^{12}} d^3 r' - \int_{\Omega_s^{\triangleleft}} \frac{\Delta N^{\triangleleft}}{|\mathbf{r} - \mathbf{r}'|^6} d^3 r', \quad (1)$$

with $\Delta M^{\triangleleft} = \rho_l^2 M_{ll} - \rho_l \rho_s^{\triangleleft} M_{sl}^{\triangleleft}$ and $\Delta N^{\triangleleft} = \rho_l^2 N_{ll} - \rho_l \rho_s^{\triangleleft} N_{sl}^{\triangleleft}$ where ρ_l and ρ_s^{\triangleleft} are the number densities of the liquid and the substrate, respectively. Because of its low density in Eq. (1) the effect of the vapor or gas phase has been neglected. The edge geometry allows one to analytically calculate both integrals in Eq. (1) which we denote as $\Pi_e^{12\triangleleft}$ and $\Pi_e^{6\triangleleft}$, respectively, so that $\Pi_e^{\triangleleft}(x, y) = \Pi_e^{12\triangleleft}(x, y) - \Pi_e^{6\triangleleft}(x, y)$.

Likewise, the contribution to the DJP of a thin coating layer of thickness d^{\triangleleft} on the upper part of an edge $\Omega_c^{u\triangleleft} = \{\mathbf{r} \in \mathbb{R}^3 \mid x \leq 0, -d^{\triangleleft} \leq y \leq 0, z \in \mathbb{R}\}$ can be determined by assuming also a van der Waals type interaction between the coating and the liquid particles, i.e., $\Pi_c^{\triangleleft}(x, y) = -\int_{\Omega_c^{u\triangleleft}} \Delta N'^{\triangleleft}/|\mathbf{r} - \mathbf{r}'|^6 d^3 r'$, with $\Delta N'^{\triangleleft} = \rho_l^2 N_{ll} - \rho_l \rho_c^{\triangleleft} N_{cl}^{\triangleleft}$ and $\Pi_c^{\triangleleft}(x \rightarrow -\infty, y) = -\pi \Delta N'^{\triangleleft} d^{\triangleleft}/(2y^4)$ [8]. As a simplification we have neglected the effect of the repulsive part of the liquid-coating interaction which gives rise to a contribution shorter ranged ($\sim y^{-10}$) than the corresponding one $\Pi_e^{12\triangleleft} \sim y^{-9}$ [20, 24]. The DJP of an edge including the coating of its upper side is $\Pi_{ce}^{\triangleleft}(x, y) = \Pi_e^{\triangleleft}(x, y + d^{\triangleleft}) + \Pi_c^{\triangleleft}(x, y)$. For $x \rightarrow -\infty$ and d^{\triangleleft} much smaller than the thickness of the wetting layer y_0^{\triangleleft} , the DJP of the coated edge reduces to that of a coated, laterally homogeneous substrate: $\Pi_{ch}^{\triangleleft}(y) = \pi \Delta M^{\triangleleft}/(45y^9) - \pi \Delta N^{\triangleleft}/(6y^3) + \pi \Delta N'^{\triangleleft} d^{\triangleleft}/(2y^4)$, with $\Delta N'^{\triangleleft} = \Delta N^{\triangleleft} - \Delta N'^{\triangleleft} = \rho_l(\rho_c^{\triangleleft} N_{cl}^{\triangleleft} - \rho_s^{\triangleleft} N_{sl}^{\triangleleft})$; $\Pi_{ch}^{\triangleleft}(y = y_0^{\triangleleft}) = 0$.

At this point we introduce dimensionless quantities (marked by a star) such that lengths are measured in units of $b^{\triangleleft} = [2\Delta M^{\triangleleft}/(15|\Delta N^{\triangleleft}|)]^{1/6}$, which for $\Delta N^{\triangleleft} > 0$ is the equilibrium wetting film thickness on the uncoated homogeneous substrate. The DJP is measured in units of σ/b^{\triangleleft} where σ is the liquid-vapor surface

tension. Thus the dimensionless DJP $\Pi_{ch}^{*\triangleleft} = \Pi_{ch} b^{\triangleleft}/\sigma$ far from the edge ($x \rightarrow -\infty$) has the following form:

$$\Pi_{ch}^{*\triangleleft}(y_*) = C^{\triangleleft} \left(\frac{1}{y_*^9} \pm \frac{1}{y_*^3} + \frac{B^{\triangleleft}}{y_*^4} \right); \quad (2)$$

in the following we drop the stars.

In Eq. (2) $B^{\triangleleft} = \pi \Delta N'^{\triangleleft} d^{\triangleleft}/(2A^{\triangleleft} b^{\triangleleft 4})$ quantifies the contribution of the coating and $C^{\triangleleft} = A^{\triangleleft} b^{\triangleleft}/\sigma$ where $A^{\triangleleft} = \pi(\Delta M^{\triangleleft}/45)^{-1/2}(|\Delta N^{\triangleleft}|/6)^{3/2}$ measures the effect of the competing intermolecular forces relative to the surface tension of the liquid-vapor interface. Since a more refined analysis of the DJP beyond Eq. (1) yields $B \neq 0$ even in the absence of a coating layer [24, 25], in the following we consider B as an independent disposable parameter. In the second term on the right hand side of Eq. (2) the upper plus (lower minus) sign corresponds to $\Delta N^{\triangleleft} < 0$ ($\Delta N^{\triangleleft} > 0$). In the following we shall refer to these cases as the plus \oplus and the minus \ominus cases, respectively. The dimensionless form of the DJP (in units of σ/b^{\triangleleft}) for a single edge coated on the upper side is given by

$$\Pi_{ce}^{\triangleleft}(x, y) = C^{\triangleleft} \left\{ \frac{45 \Pi_e^{12\triangleleft}(x, y)}{\pi \Delta M^{\triangleleft}} \pm \frac{6 \Pi_e^{6\triangleleft}(x, y)}{\pi |\Delta N^{\triangleleft}|} + \frac{2 B^{\triangleleft} [-\Pi_c^{u\triangleleft}(x, y)]}{\pi \Delta N'^{\triangleleft}} \right\}. \quad (3)$$

Here $\Pi_e^{12\triangleleft}$, $\Pi_e^{6\triangleleft}$, and $\Pi_c^{u\triangleleft}$ are measured in units of σ/b^{\triangleleft} whereas ΔM^{\triangleleft} , ΔN^{\triangleleft} , and $\Delta N'^{\triangleleft}$ are taken in units of $\sigma(b^{\triangleleft})^8$, $\sigma(b^{\triangleleft})^2$, and $\sigma(b^{\triangleleft})^2$, respectively; x and y are measured in units of b^{\triangleleft} so that C^{\triangleleft} and B^{\triangleleft} are dimensionless. The contact angle $\theta_{eq}^{\triangleleft}$ of macroscopic droplets and those values of C^{\triangleleft} and B^{\triangleleft} , which give rise to partial wetting, are related via $\cos \theta_{eq}^{\triangleleft} = 1 + \int_{y_0^{\triangleleft}}^{\infty} \Pi_{ch}^{\triangleleft}(y) dy$ with y_0^{\triangleleft} given implicitly by $\Pi_{ch}^{\triangleleft}(y_0^{\triangleleft}) = 0$ [8, 25] so that $y_0^{\triangleleft}(B^{\triangleleft} = 0) = b^{\triangleleft}$. Within these admissible ranges of values for C^{\triangleleft} and B^{\triangleleft} (see the insets of Fig. 2 in Ref. [8]), the actual contact angle of nanodroplets defined, e.g., via their slope of the point of inflection or by spherical extrapolation of their top cap towards the substrate, may differ from that of macroscopic droplets depending on the size of the nanodroplets and details of the DJP. With $q = b^{\triangleright}/b^{\triangleleft}$ the dimensionless form of the DJP for the right edge is given by

$$\Pi_{ce}^{\triangleright}(x, y) = C^{\triangleright} \left\{ \frac{45 q^9 \Pi_e^{12\triangleleft}(-x, y)}{\pi \Delta M^{\triangleleft}} \pm \frac{6 q^3 \Pi_e^{6\triangleleft}(-x, y)}{\pi |\Delta N^{\triangleleft}|} + \frac{2 q^4 B^{\triangleright} [-\Pi_c^{u\triangleleft}(-x, y)]}{\pi \Delta N'^{\triangleleft}} \right\}. \quad (4)$$

Due to the additivity of the interatomic potentials used here, the DJP of the chemical step can be obtained by superimposing the DJP of the constitutional parts, i.e., the two edges coated on the upper side. Thus the DJP of the whole substrate with a chemical step is given by $\Pi(x, y) = \Pi_{ce}^{\triangleleft}(x, y) + \Pi_{ce}^{\triangleright}(x, y)$. Figure 1 shows the contour lines of the DJP across a chemical step for a typical example.

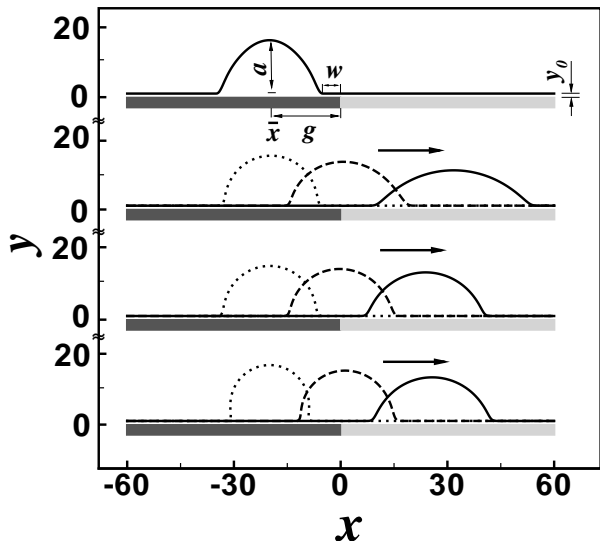


FIG. 2: The motion of a nanodroplet across three different chemical steps for the \ominus case on both sides and for $B^\triangleleft = 0$, $B^\triangleright = 0$, and $q = b^\triangleright/b^\triangleleft = 1.0$ so that $y_0^\triangleleft = y_0^\triangleright = y_0$. The uppermost part shows the initial interface profile. The parameters for the lower three parts are [$\theta_{eq}^\triangleleft = 97.2^\circ$ ($C^\triangleleft = 3$), $\theta_{eq}^\triangleright = 51.3^\circ$ ($C^\triangleright = 1$)], [$\theta_{eq}^\triangleleft = 97.2^\circ$ ($C^\triangleleft = 3$), $\theta_{eq}^\triangleright = 75.5^\circ$ ($C^\triangleright = 2$)], and [$\theta_{eq}^\triangleleft = 120^\circ$ ($C^\triangleleft = 4$), $\theta_{eq}^\triangleright = 75.5^\circ$ ($C^\triangleright = 2$)] from top to bottom. The profiles correspond to times $t = 355, 2000$, and 22025 ; $t = 375, 8125$, and 24300 ; and $t = 185, 7800$, and 23500 ; respectively, in units of $\mu b^\triangleleft / (C^\triangleleft \sigma)$. \triangleleft (\triangleright) is the less (more) wettable substrate.

In order to probe the influence of the DJP on droplets near and on chemical steps we have performed mesoscopic hydrodynamic calculations based on the two-dimensional Stokes equation. In dimensionless form the continuity and Stokes equation read $\nabla \cdot \mathbf{u} = 0$ and $C^\triangleleft \nabla^2 \mathbf{u} = \nabla p$, respectively, where $\mathbf{u} = (u_x, u_y)$ is the velocity vector and p is the hydrostatic pressure. With the viscosity μ , the velocity and time scales are taken to be $C^\triangleleft \sigma / \mu$ and $\mu b^\triangleleft / (C^\triangleleft \sigma)$, respectively. Lengths and pressure are expressed in units of b^\triangleleft and σ / b^\triangleleft , respectively. In the above Stokes equation the factor C^\triangleleft appears because its dimensionless form has been obtained by rescaling with the parameters of the left hand side of the substrate. We have solved these equations numerically with a standard biharmonic boundary integral method [26]. A no-slip boundary condition has been employed for the impermeable liquid-solid interface and it has been imposed that there is no flux through the end sides of the system. Along the liquid-vapor interface it has been assumed that the tangential stresses are zero and that normal stresses are balanced by pressure, surface tension, and the disjoining pressure, i.e., $\mathbf{n} \cdot \boldsymbol{\tau} \cdot \mathbf{n} = -p + \sigma \kappa + \Pi$ with the local curvature κ , the stress tensor $\boldsymbol{\tau}$, and the unit surface normal vector \mathbf{n} . The initial droplet shape has been taken to be a hemisphere which is smoothly connected to the wetting layer, i.e., $y(x; t = 0) = y_0^\triangleleft + a \{1 - [(|x| - g)/a]^2\}^{|x| - g|^{m+1}}$ with the droplet height a in the center equal to half the

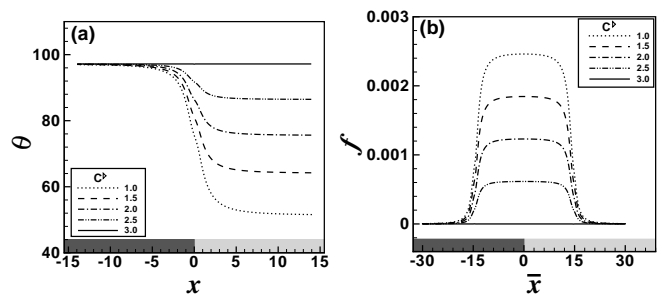


FIG. 3: (a) $\theta(x)$ and (b) dimensionless lateral force densities $f(\bar{x})$ for droplets with $a = 15$ (for \bar{x} see Fig. 2) in the vicinity of a chemical step separating two parts of the substrate with $C^\triangleleft = 3$, $B^\triangleleft = B^\triangleright = 0$, and $q = 1$. Both substrate sides correspond to the \ominus case. f is measured in units of $\sigma / (b^\triangleleft)^2$.

base width and the distance g of the droplet center from the boundary (see Fig. 2). In this study m was chosen to be 10.

We first consider the case without coating ($B^\triangleleft = B^\triangleright = 0$, which implies that ΔN is negative on both sides corresponding to the \ominus case). Numerical results for different values of C^\triangleright and C^\triangleleft are shown in Fig. 2. At time $t = 0$ droplets of height $a = 15$ have been positioned at a distance $w = 5$ (see Fig. 2) from the chemical step on the less wettable substrate. C^\triangleleft was selected such that, during the *initial* relaxation of the prepared droplet *shape*, w does not decrease. Thereafter, in all cases shown in Fig. 2 the droplets gradually move towards the more wettable side (\triangleright), as expected intuitively, and continue their motion there. This indicates that the nanodroplets can perceive the presence of the other part of the substrate over some lateral distances. As a function of time the wetting layer thickness changes slightly which is expected due to the Laplace pressure in the droplet and in view of the lateral boundary conditions on the flux.

On a homogeneous substrate, the equilibrium contact angle can be calculated from the DJP. Extending this formula, one can define a spatially varying “contact angle” via $\cos \theta(x) = 1 + \int_{y_0(x)}^{\infty} \Pi(x, y) dy$, with $\Pi(x, y_0(x)) = 0$. For $\Pi(x, y)$ rapidly varying as a function of x (e.g., in the close vicinity of a chemical step) and for very small droplets, $\theta(x)$ is not the actual contact angle, but nonetheless, as intuitively expected, $\partial_x \theta(x)$ is related to the lateral DJP induced force density (in units of $\sigma / (b^\triangleleft)^2$) acting on a droplet: $f = 1/\Omega_d \times \int_{\partial\Omega_d} \Pi(x, y) n_x dS$ where $\partial\Omega_d$ and Ω_d are the dimensionless droplet surface and volume, respectively, and n_x is the x -component of the outward surface normal \mathbf{n} . For the present purposes and for the sake of simplicity we have focused on nanodroplets large enough such that $\int_{y_0(x)}^a \Pi(x, y) dy \approx \int_{y_0(x)}^{\infty} \Pi(x, y) dy$. This means that for the types of the DJP considered in this study a is taken to be at least 10 times the thickness of the underlying wetting film. Within this range, the phenomena discussed below are largely independent of the droplet size. Since in the cases studied here the differ-

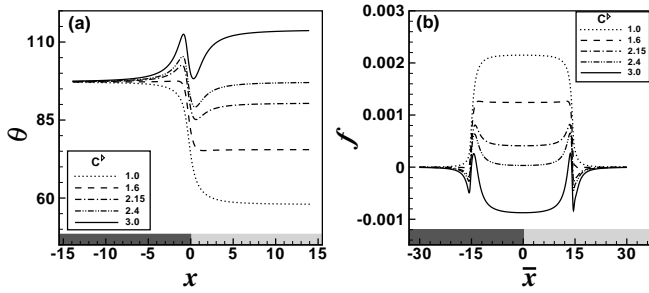


FIG. 4: (a) $\theta(x)$ and (b) dimensionless lateral force densities $f(\bar{x})$ for droplets with $a = 15$ in the vicinity of a chemical step between two substrates with $C^{\triangleleft} = 3$, $B^{\triangleleft} = B^{\triangleleft} = 0$, and $q = 1.25$. Both parts of the substrate correspond to the \ominus case. f is measured in units of $\sigma/(b^{\triangleleft})^2$.

ences in wettability between the two parts of the substrate are relatively small, in the following we have estimated $f(\bar{x})$ by considering droplets with the shape used as initial condition for the Stokes dynamics but centered at $x = \bar{x}$. For large and symmetric droplets and if $\Pi(x, y)$ varies slowly over the width of the droplet such that $\Pi(x_0 + a, y) - \Pi(x_0 - a, y) \approx 2a \partial_x \Pi(x_0, y)$, f and $-\partial\theta/\partial x$ have the same sign. Thus droplets will move towards smaller $\theta(x)$, i.e., more wettable regions.

Figure 3(a) shows $\theta(x)$ in the vicinity of the chemical step for the parameters used in Fig. 2. $\theta(x)$ monotonically decreases from $\theta_{\text{eq}}^{\triangleleft}$ to $\theta_{\text{eq}}^{\triangleleft}$ and, as shown in Fig. 3(b), the force acting on droplets of initial height $a = 15$ is positive for all positions \bar{x} of the center of the drop. The force curve has a rather flat, plateau-like shape with a maximum at $\bar{x} = 0$ and varies sharply if one of the contact lines reaches the chemical step. This result is in agreement with the numerical calculations and indicates that the droplets never come to a complete stop.

In the previous example the local contact angle $\theta(x)$ changes monotonically from $\theta_{\text{eq}}^{\triangleleft}$ to $\theta_{\text{eq}}^{\triangleleft}$. This is not necessarily the case, in particular not for steps between materials generating different thicknesses of the wetting layer, and for two substrates with different forms of the DJP, e.g., \ominus on the left and \oplus on the right side.

Figure 4 shows $\theta(x)$ and $f(\bar{x})$ for $B^{\triangleleft} = B^{\triangleleft} = 0$ and $q = 1.25$. For $C^{\triangleleft} < 1.5$, $\theta(x)$ decreases monotonically and $f(\bar{x})$ is positive for all \bar{x} . Therefore a droplet will move towards the more wettable side. For $C^{\triangleleft} = 1.6$ and larger, $\theta(x)$ is nonmonotonic. The cases between $C^{\triangleleft} = 1.6$ and 2.15 are particularly interesting because, although $\theta_{\text{eq}}^{\triangleleft} > \theta_{\text{eq}}^{\triangleleft}$, $\partial_x \theta > 0$ outside a small region around the step. A droplet is therefore expected to move towards the *less* wettable substrate. This is indeed the case because f also changes sign. Zeroes of $f(\bar{x})$ with $\partial_{\bar{x}} f(\bar{x}) < 0$ indicate that the chemical step can act as a pinning site for droplets. For $C^{\triangleleft} > 2.4$ the two parts of the substrate exchange roles in that $\theta_{\text{eq}}^{\triangleleft} < \theta_{\text{eq}}^{\triangleleft}$. Almost everywhere $f(\bar{x}) < 0$ except for those values of \bar{x} for which one of the contact lines touches the step. Thus, a droplet is expected to move towards the more wettable

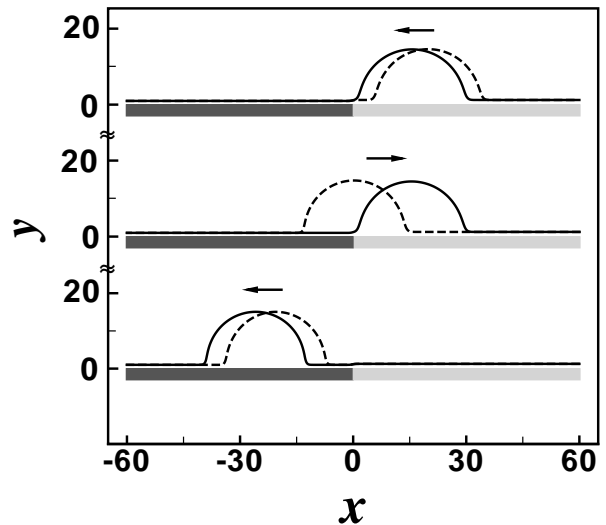


FIG. 5: Motion of a nanodroplet near a chemical step in the \ominus case on both sides, $B^{\triangleleft} = B^{\triangleleft} = 0$, $C^{\triangleleft} = 3$, $C^{\triangleleft} = 2.15$, and $q = 1.25$ (implying $\theta_{\text{eq}}^{\triangleleft} = 97.2^\circ$ and $\theta_{\text{eq}}^{\triangleleft} = 90.4^\circ$; compare Fig. 4), starting at different positions. The droplet shapes are shown, top to bottom, at $t = 170, 100$, and 45 (dashed) and at $t = 4750, 4300$, and 40000 (solid), respectively.

side. However, we expect pinning of the contact lines at the step as the droplet moves from \triangleright to \triangleleft because in this case $\partial_{\bar{x}} f(\bar{x}) < 0$ at the zeroes of $f(\bar{x})$.

In order to confirm these theoretical predictions we have performed a series of numerical calculations by positioning a nanodroplet at a distance $w = 5$ on the right hand side of the chemical step. For the case $C^{\triangleleft} = 2.15$, i.e., if the nanodroplet is initially positioned on the more wettable part of the substrate, the results of these calculations are shown in Fig. 5 for a nanodroplet with $a = 15$. This droplet moves to the left (i.e., counterintuitively towards the less wettable substrate), slows down, and stops when its advancing contact line touches the chemical step. A droplet initially spanning the step moves to the right, as expected, but stops when its receding contact line touching the step. Droplets completely located on the left part of the substrate move away from the chemical step, i.e., *away* from the *more* wettable substrate, with the velocity decreasing as the distance from the step increases. However, we do not observe a complete stop. These numerical results are in complete agreement with our analysis of the effective DJP induced force. Figure 6 shows an example for $q = 1$ in which the droplets can move towards the less wettable substrate. This is the case for different signs of the long-ranged term (here \oplus case on the left and \ominus case on the right) and for non-zero values of B (here $B^{\triangleleft} = -2.762$, $C^{\triangleleft} = 2$, and $B^{\triangleleft} = -1$). These values are chosen such that the equilibrium wetting film thicknesses are equal on both sides of the substrate. Outside a narrow region around the chemical step $\partial_x \theta(x)$ is positive everywhere. This indicates that the droplet will move to the left independent of the relative values of $\theta_{\text{eq}}^{\triangleleft}$

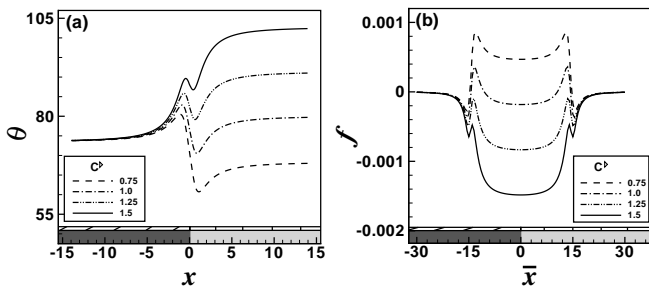


FIG. 6: (a) $\theta(x)$ and (b) dimensionless lateral force densities $f(\bar{x})$ for droplets with $a = 15$ in the vicinity of a chemical step separating two substrates (\oplus case on the left and \ominus case on the right) with $B^{\triangleleft} = -2.762$, $C^{\triangleleft} = 2$, $B^{\triangleright} = -1$, and $q = 1$ for different values of C^{\triangleright} . f is measured in units of $\sigma/(b^{\triangleleft})^2$. The different coatings of the two parts of the substrate associated with the non-zero values of B^{\triangleleft} and B^{\triangleright} are indicated in the figures.

and $\theta_{\text{eq}}^{\triangleright}$, although it will be pinned at the step if coming from the right. This is confirmed by the analysis of $f(\bar{x})$ in Fig. 6(b). If both contact lines are on the same side of the step, $f(|\bar{x}| > a) < 0$. If the droplets span the step, i.e., $|\bar{x}| < a$, the direction of the motion is towards the more wettable part of the substrate.

In all the cases we considered the direction of motion of a droplet near a chemical step (i.e., with both contact lines on the same side of the step) is determined by $\partial_x \theta(x)$. The sign of $\partial_x \theta(x)$ is the same as the sign of $-\partial_x \Pi(x, y_0(x))$. Expanding $\Pi(x, y)$ for large $|x|$ up to $O(|x|^{-3})$ one finds on both sides of the step the limiting value for a homogeneous substrate. This means that the wetting film thickness y_0 is independent of x up to this order. To leading order the gradient of the equilibrium contact angle with respect to x is the same on both sides of the chemical step and given by

$$\partial_x \theta(x) \sim \frac{3}{4|x|^3} [-(\pm q^3) C^{\triangleright} \pm C^{\triangleleft}] + \mathcal{O}(|x|^{-4}), \quad (5)$$

with the plus and minus signs in front of C^{\triangleright} and C^{\triangleleft} corresponding to the \oplus and the \ominus case on the right and the left hand side, respectively. This means that asymptotically far from the step the droplets move in the same direction on both sides of the step. For instance, for the case discussed in Fig. 4 (with $B^{\triangleleft} = B^{\triangleright} = 0$) the equilibrium contact angle can be shown to be larger on the

right side of the step if $q C^{\triangleright} > C^{\triangleleft}$, i.e., for $C^{\triangleright} > 2.4$ and the droplets move to the left for $C^{\triangleright} > C^{\triangleleft}/q^3 = 1.536$ and $|\bar{x}| > a$, in agreement with the observations.

In summary, we have outlined an approach which allows one to study in detail the behavior of nanodroplets near as well as on chemical heterogeneities. Our investigation reveals the dynamics of nanodroplets in the vicinity of chemical heterogeneities caused by long-ranged forces. We have shown that the direction of motion of the droplets is, to leading order in the distance from the step, determined by the competition of the van der Waals forces acting between the droplet and the two different materials of the substrate, i.e., the difference in the Hamaker constants (see Eq. (5)), rather than the equilibrium contact angles which depend also on the short-ranged parts of interaction potentials and on the sub-leading terms in the disjoining pressure. If the van der Waals forces direct the droplet towards the less wettable material, the droplet will stop as soon as the advancing contact line hits the step. Otherwise it will continue at a velocity rapidly decreasing with the distance from the step. Droplets which span the chemical step will move towards the more wettable substrate; however, the receding contact line can be pinned by the step.

This study demonstrates that taking into account the effect of long-ranged intermolecular forces is mandatory for accurately controlling and guiding the liquids in open nanofluidic systems. Recent experiments have shown that the arrangement of droplets on structured substrates can be explained by their crossing of chemical steps from the less wettable to the more wettable side [27]. Our study indicates that in general there can be free-energetic barriers to this process which would result in significantly altered patterns. Our analysis provides a microscopic approach to the pinning and depinning of three-phase contact lines at chemical surface heterogeneities which goes beyond the macroscopic picture of a sharp transition between regions of different wettability on a substrate [28, 29, 30, 31, 32] or the phenomenological mesoscopic approach of introducing lateral variations of the parameters entering into the effective interface potential [33].

Acknowledgment. M. R. acknowledges financial support by the Deutsche Forschungsgemeinschaft (DFG) within the priority program SPP 1164 under grant number RA 1061/2-1.

-
- [1] Karniadakis, G.; Beskok, A.; Aluru, N. *Microflows and Nanoflows: Fundamentals and Simulation*, 2nd ed.; Springer: NewYork, 2005.
- [2] Dietrich, S.; Popescu, M. N.; Rauscher, M. *J. Phys. Condens. Matter* **2005**, *17*, S577.
- [3] Daniel, S.; Chaudhury, M. K.; Chen, J. *Science* **1992**, *291*, 633.
- [4] Kusumaatmaja, H.; Yeomans, J. M. *Langmuir* **2007**, *23*, 956.
- [5] Eijkel, J. C. T.; van den Berg, A. *Microfluid Nanofluid* **2005**, *1*, 249.
- [6] Mukhopadhyay, R. *Anal. Chem.* **2006**, *78*, 7379.
- [7] Cieplak, M.; Koplik, J.; Banavar, J. R. *Phys. Rev. Lett.* **2006**, *96*, 114502.
- [8] Moosavi, A.; Rauscher, M.; Dietrich, S. *Phys. Rev. Lett.* **2006**, *97*, 236101.

- [9] Greenspan, H. P. *J. Fluid Mech.* **1978**, 84, 125.
- [10] Raphaël, E. *C. R. Acad. Sci. Paris Ser. II* **1988**, 306, 751.
- [11] Brochard, F. *Langmuir* **1989**, 5, 432.
- [12] Subramanian, R. S.; Moumen, N.; McLaughlin, J. B. *Langmuir* **2005**, 21, 11844.
- [13] Yaneva, J.; Milchev, A.; Binder, K. *J. Chem. Phys.* **2004**, 121, 12632.
- [14] Schwartz L. W.; Eley, R. R. *J. Colloid Interface Sci.* **1998**, 202, 173.
- [15] Brusch, L.; Kühne, H.; Thiele, U.; Bär, M. *Phys. Rev. E* **2002**, 66, 011602.
- [16] Pismen, L. M.; Thiele, U. *Phys. Fluids* **2006**, 18, 042104.
- [17] Zhao, Y.; Marshall, J. S. *J. Fluid Mech.* **2006**, 559, 355.
- [18] Thiele, U.; Knobloch, E. *New. J. Phys.* **2006**, 8, 313.
- [19] Koch, W.; Dietrich, S.; Napiórkowski, M. *Phys. Rev. E* **1995**, 51, 3300.
- [20] Bauer, C.; Dietrich, S. *Phys. Rev. E* **1999**, 60, 6919.
- [21] Bauer, C.; Dietrich, S. *Eur. Phys. J. B* **1999**, 10, 767.
- [22] Bauer, C.; Dietrich, S. *Phys. Rev. E* **2000**, 61, 1664.
- [23] Robbins, M. O.; Andelman, D.; Joanny, J. F. *Phys. Rev. A* **1991**, 43, 4344.
- [24] Dietrich, S.; Napiórkowski, M. *Phys. Rev. A* **1991**, 43, 1861.
- [25] Dietrich, S. in *Phase Transitions and Critical Phenomena*, edited by Domb, C.; Lebowitz, J. L.; Academic: London, 1988, p. 1.
- [26] Kelmanson, M. A. *J. Eng. Math.* **1983**, 17, 329.
- [27] Léopoldès, J.; Bucknall, D. G. *Europhys. Lett.* **2005**, 72, 597.
- [28] Casagrande C.; Fabre P.; Raphaël E.; Veyssié M. *Europhys. Lett.* **1989**, 9, 251.
- [29] Domingues Dos Santos F.; Ondarçuhu T. *J. Chim. Phys.* **1996**, 93, 1991.
- [30] Ondarçuhu T. *J. Phys. II France* **1995**, 5, 227.
- [31] Raphaël E.; de Gennes P. G. *J. Chem. Phys.* **1989**, 90, 7577.
- [32] Shanahan M. E. R. *Colloids and Surfaces A: Physiochem. Eng. Aspects* **1999**, 156, 71.
- [33] Thiele U. *Phys. Rev. Lett.* **2006**, 97, 204501.